Aqueous solvent effects on the conformational space of tryptamine. Structural and electronic analysis

Rosana M. Lobayan, María C. Pérez Schmit, Alicia H. Jubert & Arturo Vitale

ONLINE FIRST

Molecular Modeling

JOURNAL OF

Computational Chemistry
Life Science
Advanced Materials
New Methods

Springer

Springer

Springer

ORIGINAL PAPER

Aqueous solvent effects on the conformational space of tryptamine. Structural and electronic analysis

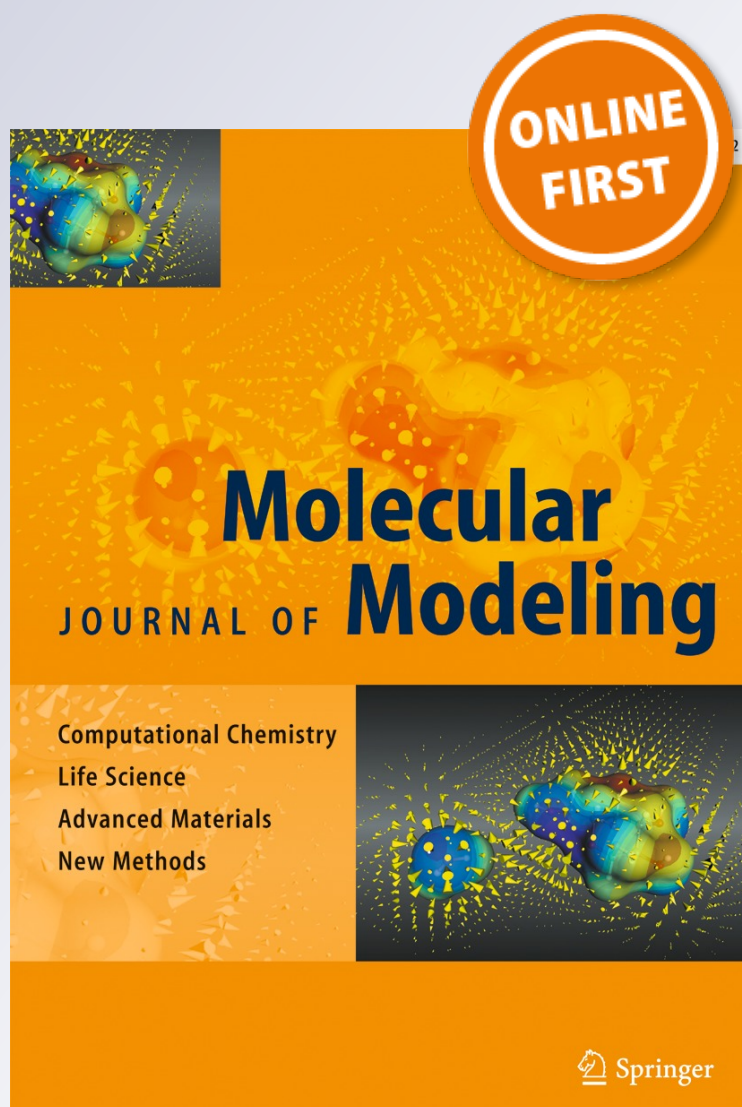**Rosana M. Lobayan · María C. Pérez Schmit · Alicia H. Jubert · Arturo Vitale**

Abstract The TRA (3-[2-aminoethyl]indole) is an important neurotransmitter with a close structural and chemical similarity to the neurotransmitter serotonin (5-hydroxytryptamine), and to melatonin (5-methoxy-*N*-acetyltryptamine), which plays a key role in daily human behavior. Moreover, TRA, and other indolic compounds are very efficient antioxidants. In this work the conformational space of TRA was scanned in aqueous solution, simulating the solvent by the polarizable continuum model.

Rosana M. Lobayan and María C. Pérez Schmit contributed equally to this work.

Electronic supplementary material The online version of this article (doi:10.1007/s00894-012-1650-6) contains supplementary material, which is available to authorized users.

R. M. Lobayan · M. C. P. Schmit
Instituto de Investigaciones Científicas (IDIC),
Facultad de Ingeniería, Universidad de la Cuenca del Plata,
Lavalle 50,
3400 Corrientes, Argentina

A. H. Jubert
CEQUINOR Facultad de Ciencias Exactas y Facultad de Ingeniería, Universidad Nacional de La Plata,
C:C: 962,
1900 La Plata, Argentina

A. Vitale
IBIMOL (ex PRALIB)(UBA, CONICET), Facultad de Farmacia y Bioquímica, Universidad de Buenos Aires,
Junín 956,
C1113AAD Buenos Aires, Argentina

R. M. Lobayan (✉)
Departamento de Física, Facultad de Ciencias Exactas y Naturales y Agrimensura, Universidad Nacional del Nordeste,
Avda. Libertad 5300,
3400 Corrientes, Argentina
e-mail: rlobayan@ucp.edu.ar

R. M. Lobayan
e-mail: rmlb@exa.unne.edu.ar

Geometry optimizations were performed at B3LYP/6-31+G** level. Electronic distributions were analyzed at a better calculation level, thus improving the basis set (6-311++G**). A topological study based on Bader's theory (atoms in molecules) and natural bond orbital (NBO) framework was performed. Structural changes found in solution were related with charge delocalization mechanisms, which explained the changes in the conformational relative population in aqueous phase. Solvent effects on molecular electrostatic potential (MEPs) were also quantified and rationalized through charge delocalization mechanisms, thus connecting changes in MEPs with changes in structure, bond polarization, orbital bonding populations, natural charges, and bond topological properties. Moreover, polarizabilities and dipolar moments were calculated. All conformers were taken into account. Our results are the first prediction of TRA polarizabilities. The results reported contribute to the understanding of the structure, stability and reactivity of TRA and other indole derivatives.

Introduction

In TRA, serotonin and melatonin the conformational flexibility of the ethylamine or *N*-acetylethylamine side chain plays an important role in its binding to receptor sites as well as its ability as radical scavenger. TRA and other indolic compounds are very efficient antioxidants, protecting both lipids and proteins from peroxidation, and it is known that the indole structure influences the antioxidant efficiency in biological systems [1–5].

In the last decades the conformational space of TRA has been studied, and experimental data on the conformers of TRA in the gas phase are widely available [6, and references cited therein]. In a previous work [7] we studied the conformational space of TRA in gas phase using molecular dynamics complemented with functional density calculations at B3LYP/6-31+G** level. The conformational preferences were explained by hyperconjugative interactions, which were revealed by NBO data. The changes of the electronic distribution introduced by the substituent and the conformational flexibility of the side chain were addressed.

Experimental complexation of tryptamine with solvent molecules such as water, methanol or ethanol were also studied [8–10]. A few theoretical studies of microhydrated complexes have been performed [6]. To our knowledge studies of solvent effects on TRA, simulating the solvent by a polarizable continuum model, have not yet been reported.

Recently, the permanent electric dipole moments of four conformers of TRA in their ground and electronically excited states using the Stark effect on their fully resolved spectra were also measured [11].

Previous theoretical results [7] on isolated molecules are very useful for determining the intrinsic properties of the system; free of any interactions, but the analysis of the molecular behavior in the presence of water is of great interest for modeling TRA in solution, and for the interaction with biological systems. With this aim, our previous results were used to evaluate the changes produced in the electronic distribution of TRA upon simulation of aqueous solvent. Therefore, this paper focuses on the analysis of aqueous solvent effects on the intrinsic electronic properties and molecular geometry. Furthermore, molecular electrostatic potential (MEPs) were obtained and thoroughly analyzed, and solvent effects on them were also quantified, and rationalized through charge delocalization mechanisms, thus connecting changes in MEPs with changes in structure, bond polarization, orbital bonding populations, natural charges, and bond topological properties.

For a deep insight on the molecular and structural properties of these compounds in biological media, the polarizabilities were also predicted, and dipolar moments were calculated. All conformers were taken into account. This knowledge will be relevant for studying in another step, other solvents, other substitution patterns, and the ability to scavenge free radicals.

Methods

The lowest-energy conformers obtained through gas phase calculations [7] were re-optimized taking into account the solvent effect by the conductor polarizable continuum model (CPCM) [12, 13] using the density functional theory (DFT), as implemented by the Gaussian 03 package [12, 14].

Geometry optimizations were performed using the Becke three-parameter hybrid functional [14, 15] combined with the Lee-Yang-Parr correlation functional [13, 15], giving rise to the well-known B3LYP method. The 6-31+G** basis set was used for all atoms. The optimized geometric structures were confirmed as minimum on the potential energy surface through an analysis of harmonic vibrational frequencies. At the same level of calculation the zero-point energy (ZPE) was obtained, which was used to correct all energy terms.

Molecular electrostatic potentials (MEP) were obtained in the van der Waals molecule surfaces using the Gaussian 03 software, and further visualized by MOLEKEL 4.0 [16].

Topological analysis and evaluation of local properties were performed by the PROAIM software [17], using wave functions calculated at the B3LYP level and the improved 6-311++G** basis set implemented in the G03 program. NBO analysis was carried out at the same level [18].

Theoretical background

In the NBO analysis, the electronic wave functions are interpreted in terms of occupied Lewis-type and unoccupied non-Lewis localized orbitals. Delocalizations of electron density between occupied Lewis-type (bond or lone pairs) NBO orbitals and formally unoccupied non-Lewis (anti-bonds or Rydberg) NBO orbitals account for stabilizing donor-acceptor interactions.

For each donor NBO (i) and acceptor NBO (j), the second order stabilization energy ($E^{(2)}$) associated with i/j delocalization is explicitly estimated by the following equation:

$$E^{(2)} = -n_i \frac{F_{ij}{}^2}{\varepsilon_j - \varepsilon_i} \qquad (1)$$

where n_i is the ith donor orbital occupancy; ε_i, ε_j, are diagonal elements (orbital energies); and F_{ij}, off-diagonal elements, respectively, associated with the Fock matrix in NBO [19].

An NBO analysis allows us also the quantification of bond polarization, donor ability and acceptor ability, and allows us to investigate which orbital interactions are mainly involved in the stability order of the observed conformers in solution.

To take into account changes on bond lengths, their topological properties, bond polarization, donor ability, acceptor ability and population of bonding orbitals, when solvent effect is considered percent values (%Δ) are obtained. The percent values take into account differences of the corresponding mean values from 12 conformers (nine of them Si-face) of TRA in solution with respect to gas phase:

$$\%\Delta x = \frac{x(solution) - x(vacuum)}{x(vacuum)} \times 100 \qquad (2)$$

A Maxwell-Boltzmann statistical average was obtained at 298.15 K of each μ cartesian component according to:

$$\langle \mu_j \rangle = \sum_i \mu_{j,i} \exp\left(-\frac{E_i}{RT}\right) \bigg/ \sum_i \exp\left(-\frac{E_i}{RT}\right) \quad (3)$$

with $j = x, y, z$, where E_i is the relative energy of the ith conformer, and $\mu_{j,i}$ is the component jth conformer. Then, obtaining the Maxwell-Boltzmann statistical average of the magnitude of the total dipole moment:

$$\langle \mu \rangle = \sqrt{\langle \mu_x \rangle^2 + \langle \mu_y \rangle^2 + \langle \mu_z \rangle^2} \quad (4)$$

The calculation of the polarizability $\langle \alpha \rangle$ was performed from:

$$\langle \alpha \rangle = \frac{1}{3}\left(\alpha_{xx} + \alpha_{yy} + \alpha_{zz}\right) \quad (5)$$

where the tensor components were obtained from the second derivatives of the energy with respect to the Cartesian components of the applied electric field ε:

$$\alpha = \left[\partial^2 E / \partial \varepsilon^2\right] \quad (6)$$

Results and discussion

The backbone of TRA consists of a heteroaromatic planar indole ring and an aminoethyl side chain (at position 3), which can adopt several distinct orientations with respect to the ring defined by three dihedral angles (δ_1: C_2—C_3—C_8—C_9, δ_2: C_3—C_8—C_9—N_{10}, δ_3: C_8—C_9—N_{10}—H_a) (Fig. 1). Variations can give rise to several different conformers. Through the study of the conformational space in solution we found 21 lowest energy conformers with C_1 symmetry,
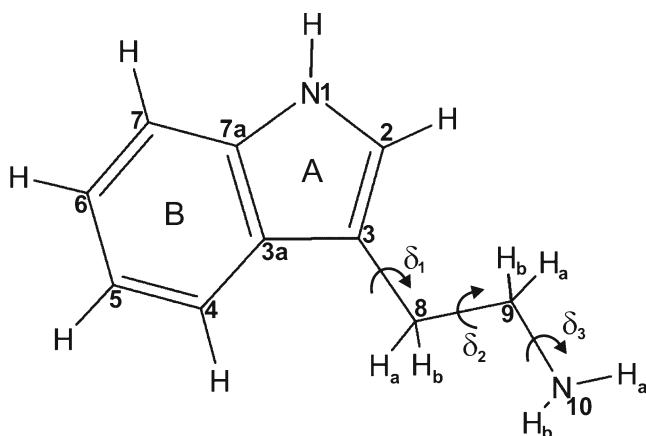

Fig. 1 Heteroaromatic planar indole ring and an aminoethyl sidechain of TRA backbone. Dihedral angles (δ_1: C_2—C_3—C_8—C_9, δ_2: C_3—C_8—C_9—N_{10}, δ_3: C_8—C_9—N_{10}—H_a) define distinct orientations of aminoethyl sidechain with respect to the ring

which in order of stability were: a) A^+TG^-/A^-TG^+, b) A^+TG^+/A^-TG^-, c) A^+TT/A^-TT, d) $A^+G^-G^-$/$A^-G^+G^+$, e) CTG^-, f) $A^+G^-G^+$/$A^-G^+G^-$, g) CTG^+, h) CTT, i) $A^+G^-G^-$/$A^-G^-G^+$, j) A^+G^+T/A^-G^-T, k) $A^+G^+G^+$/$A^-G^-G^-$ and l) CG^-T/CG^+T, (Fig. S1). They were named according to IUPAC recommendations, T, C, G+, G−, A+y A− (antiperiplanar ap: torsional angles from ±150° to 180°, synperiplanar sp: torsional angles from 0° to ±30°, synclinal+sc: torsional angles from 30° to 90°, synclinal −sc : torsional angles from −30° to −90°, anticlinal+ac: torsional angles from 90° to 150° and anticlinal −ac: torsional angles from −90° to −150°, respectively). The conformers were confirmed by the absence of imaginary frequencies in the vibrational analysis. Nine pairs of them account for structures of the same energy, but differing in the orientation of the aminoethyl group with respect to the plane of the indole ring: one of them with the aminoethyl moiety upward oriented, *Re*-face, and the other isomer having the aminoethyl moiety downward oriented, *Si*-face. Each pair shows torsion angles of opposite sign. Relevant internal coordinates of lowest energy conformers of *Re* isomers of TRA are shown in Table 1. Due to the similarity of the corresponding electronic distribution we will study only one conformer of each pair, selecting those with the aminoethyl moiety upward oriented (*Re* isomers).

The characteristics of the conformers in solution were similar to those obtained in gas phase [7] and were classified into four groups according to the position of the amino group relative to the indole ring: *gauche* on the pyrrole (group G−), *gauche* on the phenyl (group G+) or *anti* related to the indole ring (groups T (with the indole ring at right angles to the C_8—C_9 bond) and T'(with the indole ring parallel to the C_8—C_9 bond)) [7]. Conformers belonging to the same group share a common configuration relative to the C_8—C_9 bond. For example the A^+TG^-, A^+TG^+ and A^+TT conformers (group T) have in common the dihedral angle δ_2 (clinal array), with the aminoethyl group *anti* related to the indole ring (Table 1).

The difference of energy values between the structures in aqueous solvent and gas phase [7] are shown in Table 1. As expected, all structures were stabilized in solution (−13.43 kcalmol^{-1} on average). The stabilization was higher for the group T (−15.07 kcalmol^{-1} on average).

Relative conformational population at 298.15 K calculated with the Boltzmann distribution showed considerable variation in solution (Table 1). In vacuum $A^+G^-G^+$ was the most stable conformer, but in solution A^+TG^- was the most stable one. Major changes of δ_1 and δ_2 in $A^+G^-G^+$ and $A^+G^-G^-$ will be related below with charge delocalization mechanisms, thus explaining the highest stabilization of A^+TG^-, A^+TG^+ and A^+TT in solution. Moreover, within each group the up-conformers were the most stabilized (A^+TG^- conformer in group T, $A^+G^-G^-$ conformer in group G− and $A^+G^+G^-$ in group G+), which will be related with changes in δ_3 in solution.

Table 1 Energies and dihedral angles calculated at B3LYP/6-13+G** level of theory for TRA conformers[a,b,c,d]

Conformer	Vacuum Relative population (%)	ΔE (kcal mol⁻¹)	Solution Relative population (%)	ΔE (kcal mol⁻¹)	δ_1	%Δ	δ_2	%Δ	δ_3	%Δ	Δ
	$E_0 = -497.6313$ kcal mol⁻¹		$E_0 = -497.6535$ kcal mol⁻¹								
A⁺G⁻G⁺	22.73	0.00	6.12	0.82	103.2	2.7	−64.0	−1.5	64.5	2.8	−13.90
A⁺G⁻G⁻	17.63	0.15	14.02	0.33	104.3	−2.7	−62.8	−1.0	−61.1	7.4	−14.55
A⁺TG⁻	11.69	0.39	24.38	0.00	102.4	−0.5	178.5	0.1	−60.6	2.8	−15.12
A⁺TG⁺	9.61	0.51	17.84	0.19	103.7	−0.3	176.5	1.1	66.6	0.7	−15.05
A⁺TT	8.85	0.56	16.28	0.24	104.0	−1.2	−179.5	0.2	174.1	1.3	−15.04
A⁺G⁺T	8.70	0.57	1.73	1.57	95.0	−11.4	65.6	0.3	174.6	2.2	−13.72
A⁺G⁺G⁻	5.98	0.79	3.55	1.14	86.6	−3.3	61.8	0.2	−57.6	−4.0	−14.37
CTG⁻	4.55	0.95	6.89	0.75	0.0	−0.9	180.0	0.0	−59.6	2.4	−14.93
CGT	3.81	1.06	0.45	2.36	30.1	−84.6	−66.5	−5.6	179.3	−0.2	−13.42
CTG⁺	3.02	1.19	4.26	1.03	−2.3	−32.7	179.0	−0.2	66.3	0.9	−14.85
CTT	3.02	1.19	4.02	1.07	2.3	79.7	−179.0	−0.1	174.5	1.7	−14.88
A⁻G⁻G⁺	0.02	2.39	0.46	2.36	114.6	−27.1	83.3	−25.2	74.4	−15.8	−14.75

[a] Energies corrected for zero point energy (ZPE)

[b] ΔE represents the difference of energy between the most stable conformer (A⁺ G⁻ G⁺) and each of the remaining conformers

[c] %Δ represents the percentage values of changes for angles in solution with respect to vacuum

[d] Δ represents the difference of energy values between the structures in aqueous solvent and gas phase

Topology of the electronic charge density function and NBO analysis

AIM theory is based on the analysis of critical points (CPs) of the molecular charge density, ρ. At these points, the gradient of the electronic density, $\nabla\rho$, is null, and it is characterized by the three eingenvalues, λ_i (i=1,2,3), of the $\nabla^2\rho$ Hessian matrix. The CPs are named and classified as (r,s) according to their rank, r (number of non-zero eingenvalues), and signature, s (the three eingenvalues algebraic sum). Several properties evaluated at the bond CP (BCP) (a (3,-1) CP) constitute powerful tools to classify a given chemical structure: the values of electron charge density (ρ_b), Laplacian of charge density ($\nabla^2\rho_b$), Hessian matrix eigenvalues (λ_1, λ_2 and λ_3), ellipticity (ε), kinetic energy density (G_b), and the $|\lambda_1|/\lambda_3$ and G_b/ρ_b relationships [20].

All the BCPs of TRA were characterized by large ρ_b values, significant and less than zero $\nabla^2\rho_b$ values, ($|\lambda_1|/\lambda_3$)>1 and G_b/ρ_b<1 (Table S1), which means that negative curvatures predominate, and electron charge is locally concentrated within the interatomic region, thus leading to interactions typical for covalent bonds. In vacuum similar findings were found [7].

The AIM analysis allowed us to identify and characterize intramolecular hydrogen bonding (HB) interaction $N_{10}\cdots H—C_2$ in CG^-T conformer as was found in vacuum [7]. This H-bond closes a six-membered ring, accompanied by the appearance of ring critical points (RCPs), as required to fulfill the Poincaré-Hopf relationship [20]. This HB was described by relatively low ρ_b values (0.007 a.u.), $\nabla^2\rho_b$>0 (0.025 a.u.), $|\lambda_1|/\lambda_3$<1 (0.111) and G_b/ρ_b<1 (0.773) and was classified as closed shell interaction. A decrease in 38.8 % of ρ_b value was found in solution, thus showing an HB interaction of lower strength in aqueous phase [7]. Moreover, a high value of ε (3.689 in solution, and 0.199 in vaccum) indicates a BCP near to coalesce with the corresponding RCP, which means bond breakdown [20], thus indicating a lower stability for this interaction in solution.

It is worth mentioning that the HB interaction $N_{10}\cdots H—C_4$ found in vacuum for $A^+G^+G^+$ [7] was not found in solution. Higher variation in δ_1, δ_2 and δ_3 found for $A^+G^+G^+$ in solution explained this result.

The sums of second order stabilization energies ($E^{(2)}$, Eq. 1) related to bonds of the side chain: $C_3—C_8$, $C_8—C_9$, $C_9—N_{10}$, $C_9—H_b$, and the lone pair of N_{10} (LP_{N10}) are shown in Table 2. Charge delocalization effects are therefore described, thus explaining the stability order of the mentioned conformers. Orbital interactions involving LP_{N10} were relevant ($LP_{N10}\rightarrow\sigma^*$); in fact, in $A^+G^+G^-$, A^+G^+T, $A^+G^+G^+$ and CG^-T conformers those were enough to explain the stability order. The charge transfer in which the lone pair delocalizes toward a *trans* bonding orbital was always the relevant one. The higher values were found in

Table 2 Summation of second-order stabilization energies, $E^{(2)}$, of relevant donors for TRA conformers calculated at the B3LYP/6-311++G** level of theory [a,b]

Donor $\Sigma E^{(2)}$	A^+TG^-	A^+TG^+	A^+TT	$A^+G^-G^-$	CTG^-	A^+G^-T	CTG^+	CTT	$A^+G^-G^+$	A^+G^+T	$A^+G^+G^+$	CG^-T
LP_{N10}	11.22 (−8.41)	9.12 (−7.79)	9.08 (−7.44)	11.57 (−8.17)	11.06 (−7.91)	9.21 (−7.99)	8.98 (−8.74)	8.97 (−8.84)	11.71 (−8.08)	9.30 (−8.46)	9.06 (−5.23)	8.59 (−13.76)
$\sigma_{C3—C8}$	10.29 (9.35)	8.98 (−0.77)	8.64 (−0.58)	9.08 (9.27)	9.84 (−0.81)	9.08 (−1.41)	9.51 (−0.84)	9.50 (−0.73)				
Σ							18.49	18.47				
$\sigma_{C8—C9}$	4.78 (−1.65)	6.24 (−4.73)	6.13 (−4.37)	4.81 (−3.41)	4.57 (1.11)	6.33 (−5.10)						
Σ					25.47	24.62						
$\sigma_{C9—N10}$	0.88 (3.62)	1.08 (1.17)	1.43 (0.00)	1.13 (0.00)								
Σ				26.59								
$\sigma_{C9—Hb}$	6.53 (−6.69)	6.50 (−6.56)	3.51 (2.65)									
Σ	33.7	31.92	28.79									

[a] All values are expressed in kcal mol^{-1}

[b] Values within parenthesis are the percentage values of changes for summation of $E^{(2)}$ in solution with respect to the summation of $E^{(2)}$ in vacuum (%Δ)

up conformers $A^+G^+G^-$, $A^+G^-G^-$ and A^+TG^-, and were related to charge transfers where the *trans* bonding orbital (acceptor orbital) accounts for a C—C bond ($\sigma^*_{C—C}$). The remaining conformers showed lower values because the *trans* bonding orbital corresponds to a C—H bond ($\sigma^*_{C—H}$), thus showing C—C antibonding orbitals as better acceptors than C—H antibonding orbitals according to previous reports [19]. The same trend was found in vacuum [7]. In the following five conformers the consideration of charge transfers from C_3—C_8 (CTG$^+$ and CTT conformers), C_8—C_9 (A^+G^+T and CTG$^-$ conformers) and C_9—N_{10} ($A^+G^-G^-$ conformer) bonding orbitals was also needed to explain their stability. Finally, in A^+TG^-, A^+TG^+ and A^+TT conformers the transfers from C_9—H_b bonding orbital were also required.

NBO analysis of solvent effects on the conformer stability order

As shown above, the stability order found in vacuum was modified in solution. In the following paragraphs we will analyze charge delocalization mechanisms that explain the changes defining the relative population of conformers in solution.

Relevant NBO second-order stabilization energies for the group T (A^+TG^-, A^+TG^+ and A^+TT conformers) are shown in Table 3. Charge transfers related to electronic delocalization between indole backbone and aminoethyl moiety are reported. The strongest charge delocalization in A^+TG^- was found, which explained their higher stability in solution. Charge transfers related to LP_{N10} followed the stability order within a group (Tables 2 and 3), which was not found in vacuum [7]. This finding was also observed for the other groups (Tables S2a, S2b and S2c) and was associated with larger changes measured in δ_3 in solution for up-conformers. These results showed the relevance of LP_{N10} for the description of the structure stabilization in solution.

Although in both group T and $A^+G^-G^+$ and $A^+G^-G^-$ conformers a decrease in charge transfer $\sigma_{C8—C9} \rightarrow \pi^*_{C2—C3}$ was found in solution, the decrease was lower in group T (-3.35 %, -4.17, -1.97 for A^+TG^-, A^+TG^+ and A^+TT, respectively, and -7.69 % and -6.57 % for $A^+G^-G^+$ and $A^+G^-G^-$, respectively; Table S2b). We relate these results with the changes in δ_1, which were minor in group T (Table 1). Moreover, for

Table 3 Second-order stabilization energies, $E^{(2)}$, calculated at the B3LYP/6-311++G** level of theory for donation transferences in solution related to the group T[a,b]

Donor	Acceptor	Group T					
		A^+TG^-	%Δ	A^+TG^+	%Δ	A^+TT	%Δ
LP_{N10}	$\sigma^*_{C3—C8}$	0.75	−3.85	-	-	-	-
	$\sigma^*_{C8—C9}$	7.95	−6.58	0.96	−16.52	0.94	−16.81
	$\sigma^*_{C9—Ha}$	1.29	−16.20	7.19	−6.26	1.00	−8.26
	$\sigma^*_{C9—Hb}$	1.23	−13.40	0.97	−9.35	7.14	−5.93
$\sigma_{C3a—C3}$	$\sigma^*_{C3—C8}$	1.76	27.54	1.39	2.21	1.35	2.27
$\sigma_{C2—C3}$	$\sigma^*_{C3—C8}$	2.16	16.76	1.82	−1.09	1.82	−1.62
$\pi_{C2—C3}$	$\sigma^*_{C8—C9}$	3.82	2.41	3.72	2.48	3.73	2.47
$\sigma_{C3a—C7a}$	$\sigma^*_{C3a—C3}$	1.57	9.03	1.46	1.39	1.05	0.96
$\sigma_{C3—C8}$	$\sigma^*_{C3a—C7a}$	1.62	3.85	1.57	0.00	1.16	0.87
	$\sigma^*_{C9—N10}$	2.40	4.80	1.97	1.55	1.95	2.09
$\sigma_{C8—C9}$	$\pi^*_{C2—C3}$	2.60	−3.35	2.53	−4.17	2.49	−1.97
	$\sigma^*_{C3—C8}$	0.90	0.00	0.82	3.80	0.82	5.13
$\sigma_{C8—Ha}$	$\sigma^*_{C2—C3}$	3.61	1.40	3.51	−0.57	3.54	2.61
$\sigma_{C9—Ha}$	$\sigma^*_{N10—Ha}$	3.05	−9.76	-	-	-	-
	$\sigma^*_{N10—Hb}$	-	-	-	-	2.96	−10.03
$\sigma_{C9—Hb}$	$\sigma^*_{N10—Ha}$	-	-	2.95	−10.33	-	-
	$\sigma^*_{N10—Hb}$	3.05	−9.76	-	-	-	-
$\sigma_{C9—N10}$	$\sigma^*_{C3—C8}$	1.38	3.62	1.71	1.17	1.75	0.00
$\sigma_{N10—Ha}$	$\sigma^*_{C8—C9}$	-	-	-	-	2.77	6.54
	$\sigma^*_{C9—Ha}$	2.46	5.58	-	-	-	-
	$\sigma^*_{C9—Hb}$	-	-	2.32		-	-
$\sigma_{N10—Hb}$	$\sigma^*_{C8—C9}$	-	-	2.78	6.51	-	-
	$\sigma^*_{C9—Ha}$	-	-	-	-	2.35	5.38
	$\sigma^*_{C9—Hb}$	2.42	5.22	-	-	-	-
Σ		44.02		37.67		36.82	

[a] All values are expressed in kcal mol^{-1}

[b] %Δ represents the percentage values of changes for $E^{(2)}$ in solution with respect to vacuum

A^+TG^- increased transfers from the bonding orbital σ_{C9-N10} to the antiperiplanar antibonding orbital ($\sigma_{C9-N10} \rightarrow \sigma^*_{C3-C8}$: 3.62 %) was found (Table 3). Instead, the equivalent charge transfer in $A^+G^-G^+$ ($\sigma_{C9-N10} \rightarrow \sigma^*_{C8-Ha}$) decreased in solution (−5.04 %; Table S2b). For $A^+G^-G^-$ a decrease of $\sigma_{C9-Ha} \rightarrow \sigma^*_{C8-Hb}$, $\rightarrow \sigma^*_{N10-Ha}$ and $\sigma_{C9-Hb} \rightarrow \sigma^*_{N10-Hb}$ was found (−3.20 %, −8.36 %, −6.01 %, respectively; Table S2b). These results may be related to major changes in δ_2 experienced by $A^+G^-G^+$ and $A^+G^-G^-$ in solution (Table 1, Fig. 1). Therefore, our results showed that the lower decrease in solution of $\sigma_{C8-C9} \rightarrow \pi^*_{C2-C3}$ and $\sigma_{C9-N10} \rightarrow \sigma^*_{C3-C8}$ charge delocalizations for group T with respect to the values for $A^+G^-G^+$ and $A^+G^-G^-$ conformers explained the major stabilization of group T in solution.

AIM/NBO analysis of solvent effects on chemical bonds

Table 4 shows values in vacuum for bond lengths, electron density at NCP of hydrogen atom (ρ_{H-NCP}), electron density at BCPs (ρ_b), ellipticity (ε), bond polarization, donor ability, acceptor ability and population of C—H and N—H bonding orbitals belonging to indole ring, and percent values (%Δ) of the changes when solvent effect is considered (Eq. 2). The percent values take into account differences of the mean values from 12 conformers (nine of them Si-face) of TRA in solution with respect to gas phase.

For indole ring we found:

i)   For N_1—H bond: Increase in bond length (1.56 %), bond polarization (3.39 %) and increase in the sum of $E^{(2)}$ for charge transfers from σ_{N1-H} bonding orbital (10.36 %), which is a measure of their increased donor ability. Decrease in ρ at BCP (−4.29 %) and at NCP of H_1 (−5.60 %) and decrease in the sum of $E^{(2)}$ for charge transfers to σ^*_{N1-H} antibonding orbital (−11.87 %), which is a measure of their decreased acceptor ability.

ii) For C—H bond: Increase in bond length (0.28 %), bond polarization (1.35 %) and donor ability (2.47 %). Decrease in the acceptor ability (−2.41 %) and decrease in ρ at BCP (from −0.03 % to −0.48 %) and at NCP of H (from −0.92 % to −1.30 %). For C_4—H bond a decrease in donor ability was found (−2.10 %).

iii) For LP_{N1}: Increase in donor ability (7.86 %).

For side chain we found (Table S3):

iv) For N_{10}—$H_{a/b}$ bond: Increase in bond length (0.57 %), bond polarization (1.37 %) and donor ability (3.74 %). Decrease in acceptor ability (−6.99 %) of ρ at BCP (−1.25 %) and at NCP of $H_{a/b}$ (−1.71 %).

v)   For C—H bond: Slight changes depending on the studied conformer.

vi) For LP_{N10}: Decrease in donor ability (−8.38 %).

X—H bonds belonging to indole ring were greatly affected in solution.

Moreover, we found:

vii) Increase in ε for N_1—C_{7a} (6.82 %) and C_3—C_{3a} (3.33 %) bonds with increases for $\sigma_{N1-C2} \rightarrow \sigma^*_{C7a-C7}$, $\sigma_{C2-C3} \rightarrow \sigma^*_{C3a-C4}$ and $\sigma_{C3-C8} \rightarrow \sigma^*_{C3a-C7a}$ charge transfers (values for group T are shown in Tables 3 and 5).

Molecular electrostatic potential

The molecular electrostatic potential (MEP) has been used extensively to predict the behavior and reactivity of a wide variety of chemical systems [21–23]. The potentials, created in the space around a molecule by its nuclei and electrons, are a useful tool for the study of molecular reactivity. Unlike other current parameters used as reactivity indices, $V(r)$ is an actual physical property that can be determined experimentally and by computational methods. The calculation of physicochemical properties on the molecular surface, and its visualization by a color code allows a different view of molecular behavior.

We used herein the procedure proposed by Politzer et al. [21] to predict targeted sites for electrophilic attack in the regions of negative $V(r)$ values. Moreover, the study was enriched by a thorough analysis of molecular electrostatic potential, in light of the complementarity of the different theoretical tools used to rationalize other aspects of their distribution [7, 24–27].

MEPs for A^+TG^- conformer in gas phase and in aqueous phase are shown in Fig. 2. In all conformers in both gas phase [7] and aqueous phase there were three main sites of electrophilic attack associated with C_5, N_1 and N_{10} atoms. MEPs for $A^+G^-G^-$, A^+G^-T and $A^+G^+G^+$ are also shown in Fig. 3.

In order to explain the reactivity at C_5, the population of bonding orbitals was studied. Changes in bonding orbital populations in a.u. are shown in Fig. 4. Our results showed higher population for σ_{C4-C5} and σ_{C5-C6} bonding orbitals (1.9806 and 1.9811, respectively for A^+TG^-) than for σ_{C3a-C4}, σ_{C6-C7} and σ_{C7-C7a} (1.9771, 1.9782 and 1.9784, respectively for A^+TG^-) in solution. The populations of σ_{C4-C5} and σ_{C5-C6} bonding orbitals (1.9787 and 1.9805, respectively for A^+TG^-) were also higher than those of σ_{C3a-C4}, σ_{C6-C7} and σ_{C7-C7a} bonding orbitals in vacuum (1.9752, 1.9777 and 1.9781, respectively for A^+TG^-). These results explained the increased reactivity at C_5 site found by the MEP analysis.

It is worth noting the effect of solvent on the population of the other bonds; they are studied taking A^+TG^- conformer as a sample compound. Similar trends were found in the other conformers.

Population of the C—H and C—N bonding orbitals decreased, and population of the C—C bonding orbitals of the rings increased (Fig. 4). Changes in natural charges are shown in Fig. 5. Decreased charges at H atoms, and

Table 4 Vacuum values for bond lengths, electron density at NCP of hydrogen atom (ρ_{H-NCP}), electron density at BCPs (ρ_b), ellipticity (ε), bond polarization, donor ability, acceptor ability and population of C—H and N—H bond orbitals belonging to indole ring and percentage values (%Δ) of the changes of these values when the solvent effect is considered, calculated at B3LYP/6-311+ +G** level of theory for TRA conformers[a,b]

	Bond	Bond length		ρ_{H-NCP} [c]		ρ_b		ε		Polarization[d]		Donor ability		Acceptor ability		Population	
		$x_{(vacuum)}$	%Δ	$x_{(vacuum)}$	%Δ	$x_{(vacuum)}$	%Δ	$x_{(vacuum)}$	%Δ	$x_{(vacuum)}$	%Δ	$x_{(vacuum)}$	%Δ	$x_{(vacuum)}$	%Δ	$x_{(vacuum)}$	%Δ
Ring A	N_1—H	1.007	1.56	0.433	-5.60	0.340	-4.29	0.051	-14.00	70.60	3.39	3.71	10.36	8.55	-11.87	1.6485	-0.05
	C_2—H	1.081	0.31	0.439	-1.30	0.283	-0.29	0.044	-9.56	60.46	1.63	6.70	1.18	8.61	-4.51	1.6552	-0.03
	N_1—C_{7a}	1.380	-0.19	-	-	0.300	1.24	0.120	6.82	61.50	-0.62	10.18	-0.79	15.42	-1.17	1.9862	0.00
	N_1—C_2	1.386	-0.22	-	-	0.295	1.10	0.152	-5.65	62.72	-0.29	11.91	-3.95	5.92	-9.63	1.9845	-0.01
	C_2—C_3	1.376	0.21	-	-	0.319	-0.65	0.345	-2.24	51.38	-2.83	36.49	0.58	38.61	-1.11	1.9741	0.00
	C_3—C_{3a}	1.446	-0.04	-	-	0.279	0.01	0.170	3.33	49.16	-0.68	21.40	-1.07	23.06	0.82	1.9643	0.02
	C_{3a}—C_{7a}	1.423	0.27	-	-	0.298	-0.68	0.201	-1.38	50.61	-0.31	79.17	-1.16	71.61	-0.17	1.9598	0.06
Ring B	C_4—H	1.086	0.28	0.441	-0.88	0.280	-0.48	0.021	3.94	60.48	0.98	9.54	-2.10	7.12	-2.46	1.6485	-0.01
	C_5—H	1.086	0.27	0.443	-0.92	0.280	-0.39	0.026	3.48	60.23	1.11	8.38	3.35	5.91	-0.35	1.6552	-0.02
	C_6—H	1.086	0.27	0.443	-0.97	0.280	-0.37	0.023	4.79	60.21	1.23	8.17	2.16	5.92	-1.28	1.4509	-0.04
	C_7—H	1.087	0.25	0.440	-1.25	0.278	-0.03	0.026	-5.35	60.35	1.82	9.48	3.20	6.86	-3.43	1.6452	-0.02
	C_{3a}—C_4	1.408	0.16	-	-	0.299	-0.48	0.182	-0.63	51.76	-0.49	14.25	-3.16	20.63	-0.24	1.9753	0.05
	C_4—C_5	1.391	0.15	-	-	0.309	-0.49	0.236	-0.35	50.12	0.43	49.19	-3.68	46.90	0.51	1.9796	0.04
	C_5—C_6	1.412	0.21	-	-	0.298	-0.63	0.192	-1.26	50.13	-0.12	10.41	-2.79	11.94	2.09	1.9806	0.02
	C_6—C_7	1.391	0.19	-	-	0.308	-0.35	0.239	-1.44	49.23	0.20	49.81	-1.26	47.69	-1.47	1.9777	0.03
	C_7—C_{7a}	1.400	0.16	-	-	0.303	-0.37	0.215	-2.80	48.35	-0.03	12.79	-3.67	19.55	2.56	1.9780	0.02

[a] %Δ represents the percentage difference relative to TRA average values in solution with respect to vacuum (Eq. 2)

[b] ρ_{H-NCP} and ρ_b are expressed in a.u. and bond lengths in Å

[c] Electron density at NCP of hydrogen atom

[d] Polarization of X—H bond (X = C, N), % of electron density at H atom

Table 5 Percentage values of the main changes for second-order stabilization energies, $E^{(2)}$, calculated at B3LYP/6-311++G** level of theory for donation and back-donation transferences related to A and B rings in the group T [a,b]

Donation		A^+TG^-			A^+TG^+			A^+TT		
Ring A	Ring B	Vacuum	Solution	%Δ	Vacuum	Solution	%Δ	Vacuum	Solution	%Δ
σ_{C3a-C3}	σ^*_{C4-C5}	1.46	1.55	6.16	1.46	1.48	1.37	1.90	1.91	0.53
σ_{C2-C3}	σ^*_{C3a-C4}	5.71	5.99	4.90	5.69	5.89	3.51	5.17	5.33	3.09
π_{C2-C3}	$\pi^*_{C3a-C7a}$	15.68	16.37	4.40	15.65	16.36	4.54	14.12	14.71	4.18
$\pi_{C3a-C7a}$	π^*_{C4-C5}	19.76	20.07	1.57	19.74	20.06	1.62	20.31	20.54	1.13
	π^*_{C6-C7}	18.73	18.79	0.32	18.76	18.79	0.16	18.90	18.91	0.05
σ_{N1-C2}	σ^*_{C7a-C7}	4.95	5.11	3.23	4.95	5.11	3.23	4.87	5.03	3.29
σ_{N1-C7a}	σ^*_{C3a-C4}	2.58	2.69	4.26	2.57	2.59	0.78	2.51	2.54	1.20
	$\sigma^*_{C3a-C7a}$	0.71	0.74	4.23	0.71	0.73	2.82	0.85	0.87	2.35
	σ^*_{C7a-C7}	1.54	1.60	3.90	1.54	1.60	3.90	1.53	1.58	3.27
	σ^*_{C6-C7}	1.06	1.10	3.77	1.06	1.08	1.89	1.08	1.09	0.93
	Σ	72.18	74.01	36.74	72.13	73.69	23.82	71.24	72.51	20.02
Back-donation		A^+TG^-			A^+TG^+			A^+TT		
Ring B	Ring A	Vacuum	Solution	%Δ	Vacuum	Solution	%Δ	Vacuum	Solution	%Δ
σ_{C4-C5}	σ^*_{C3a-C3}	5.16	4.78	−7.36	5.16	5.18	0.39	4.13	4.16	0.73
σ_{C3a-C4}	σ^*_{C2-C3}	0.98	0.88	−10.20	0.99	0.96	−3.03	1.20	1.18	−1.67
$\pi_{C3a-C7a}$	π^*_{C2-C3}	18.83	18.23	−3.19	18.81	18.21	−3.19	19.25	18.73	−2.70
π_{C4-C5}	$\pi^*_{C3a-C7a}$	16.89	16.33	−3.32	16.89	16.33	−3.32	15.04	14.62	−2.79
π_{C6-C7}		18.75	18.26	−2.61	18.73	18.27	−2.46	18.21	17.81	−2.20
σ_{C7a-C7}	σ^*_{N1-C2}	1.65	1.66	0.61	1.65	1.64	−0.61	1.67	1.66	−0.60
σ_{C3a-C4}	σ^*_{N1-C7a}	2.00	1.98	−1.00	2.01	1.96	−2.49	2.37	2.32	−2.11
$\sigma_{C3a-C7a}$		0.52	-	-	0.52	0.51	−1.92	0.55	0.54	−1.82
σ_{C7a-C7}		1.40	1.43	2.14	1.40	1.45	3.57	1.42	1.47	3.52
σ_{C6-C7}		6.39	6.26	−2.03	6.39	6.26	−2.03	6.33	6.22	−1.74
	Σ	72.57	69.81	−26.96	72.55	70.77	−15.09	70.17	68.71	−11.38

[a] All values are expressed in kcal mol^{-1}

[b] %Δ represents the percentage values of changes for $E^{(2)}$ in solution with respect to vacuum

increased charges at C atoms of B and A rings were found, except for C_3. These results were related with the (i), (ii) and (iv) charge delocalization mechanisms, which take charge from C—H bonds, N—H bonds and sidechain (Table 3) to A and B rings (see dashed arrows in Fig. 6).

Solvent effects on MEPs at NH and CH chemical bonds

Other solvent effects on N—H and C—H bonds for A^+TG^- are shown in Fig. 7; bond lengths, electron density at BCPs, electron density at NCPs, bond polarization, donor ability and acceptor ability are reported.

According to (i) for N_1—H bond of A^+TG^-, increased bond length, polarization, and donor ability were found (1.57 %, 3.38 %, 9.65 %, respectively; Fig. 7) in solution. Also decreased electron densities at N_1—H BCPs and H NCPs were found (−4.29 % and −5.60 %; Fig. 7). These features were associated with an increase in V(r) at H atom (27.22 % for

A^+TG^-; Fig. 2). Interestingly, these results correlated with higher changes in natural charges at H_1 atom as shown in Fig. 5.

According to (iv) for N_{10}—$H_{a/b}$ bonds of A^+TG^-, increased bond lengths, polarization, and donor ability were also found (0.61 %, 1.58 %, 5.40 %, respectively; Fig. 7) in solution. Also decreased electron densities at N_{10}—$H_{a/b}$ BCPs and $H_{a/b}$ NCPs were found (−1.33 % and −1.86 %, respectively; Fig. 7). The trends were the same as for N_1—H, but the changes were lower. These features were related with an increased region of higher values of V(r) at $H_{a/b}$ atoms (Fig. 2), and also correlated with the changes (decrease) in solution of natural charges of $H_{a/b}$ (Fig. 5).

According to (ii) and (v) the behavior of C—H bonds of A^+TG^- depends on their position in the molecular system.

The C—H bonds belonging to the aromatic ring were highly affected in solution, increased bond lengths, polarization, and donor ability were also found (0.27 %, 0.82 %, 4.70 %, respectively for A^+TG^-; Fig. 7). Also decreased
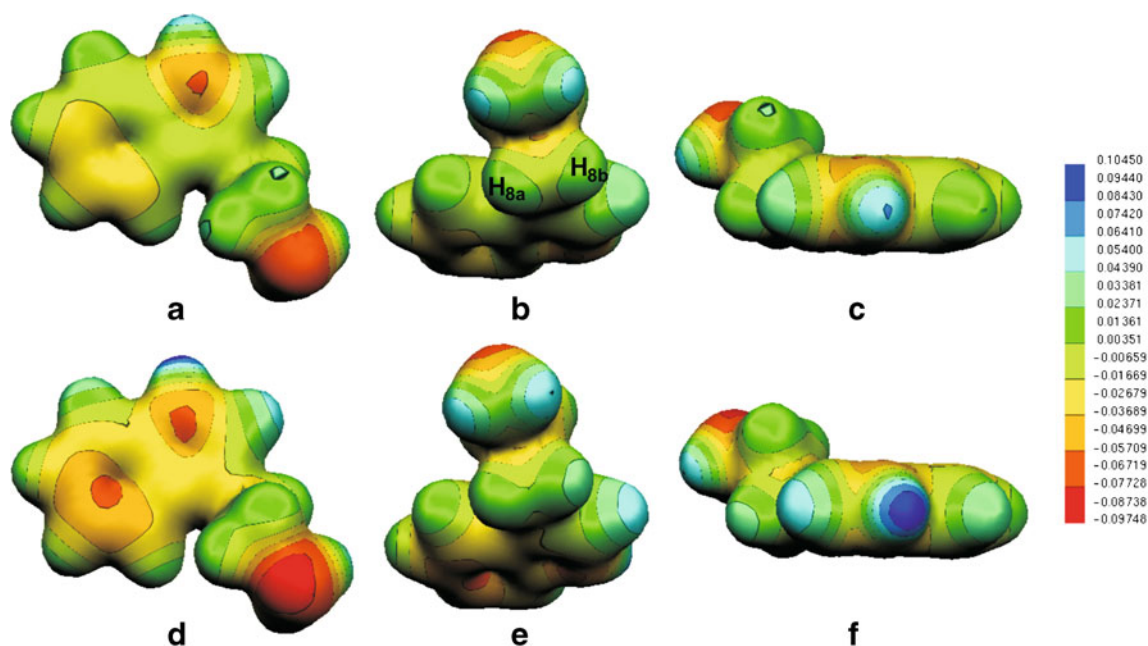
Fig. 2 Molecular electrostatic potential (MEP) for A$^+$TG$^-$ conformer of TRA in gas phase (**a**)-(**c**) and water solution (**d**)-(**f**)

electron densities at C—H BCPs and H NCPs were found in solution (−0.29 % and −1.30 % for A$^+$TG$^-$; Fig. 7). These features were related with an increase in V(r) at H atoms (Fig. 2), and also correlated with the decrease in their natural charges in solution (Fig. 5).

The C—H bonds belonging to the side chain showed slight changes, but it is interesting to note the effect of the solvent at each H atom in CH$_2$ moieties.

In C$_8$—H$_{a/b}$ moiety V(r) was similar at both hydrogen atoms in solution, but was higher in H$_{8b}$ than in H$_{8a}$ in solution (Fig. 2). The increase in V(r) at H$_{8b}$ (59.75 %)

correlated with a relative increase in the donor ability of C$_8$—H$_b$ bonding orbital. In fact, E$^{(2)}$ sums for charge transfers from $\sigma_{C8—Hb}$ bonding orbital increased in 1.51 %, and sums from $\sigma_{C8—Ha}$ bonding orbital increased in 0.35 %. We also found an increase in C$_8$—H$_b$ bond polarization (0.73 %) and a decrease in electron density at H$_{8b}$ NCP (−0.31 %), (Fig. 7 and Table S3). Bond lengths and electron density at BCP changed slightly following N—H trends.

In C$_9$—H$_{a/b}$ moiety a V(r) decrease at both H atoms was found in solution. Consequently, we found decreased donor ability of C$_9$—H$_{a/b}$ bonding orbitals. In fact, E$^{(2)}$ sums for
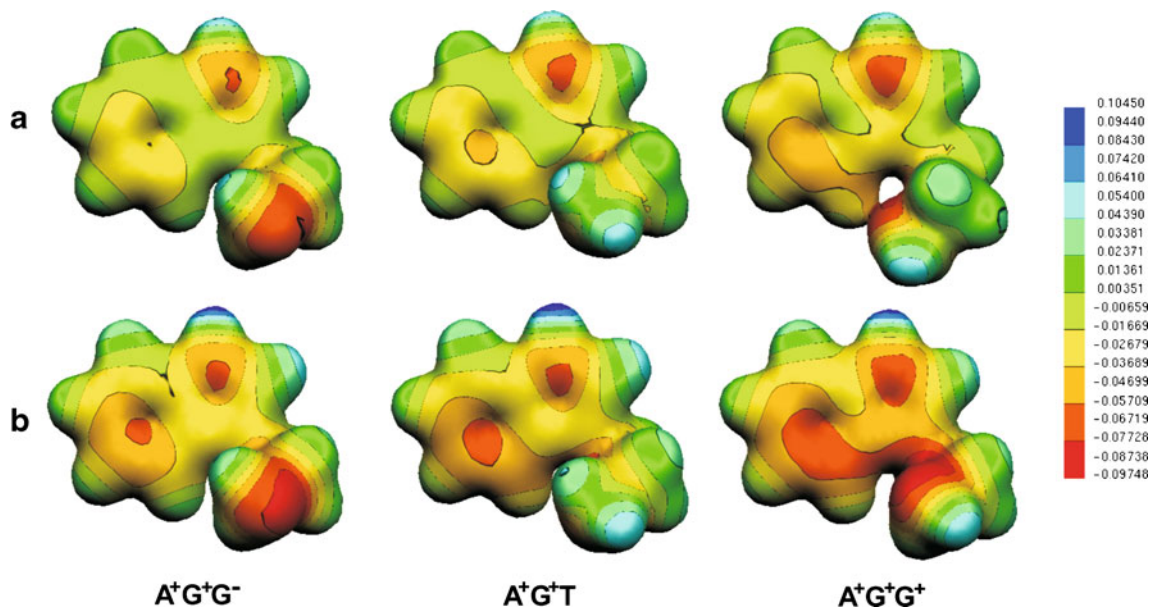

Fig. 3 Molecular electrostatic potential (MEP) for A$^+$G$^+$G$^-$, A$^+$G$^+$T and A$^+$G$^+$G$^+$ conformers of TRA in gas phase (**a**) and water solution (**b**)

Fig. 4 NBO analysis of natural population of bonding orbitals for A^+TG^- conformer in vacuum (values in parenthesis account for the difference of natural population values between the structures in aqueous solvent and gas phase). Values within the boxes correspond to natural population of lone pairs. Populations of natural bonding orbitals are given in a.u
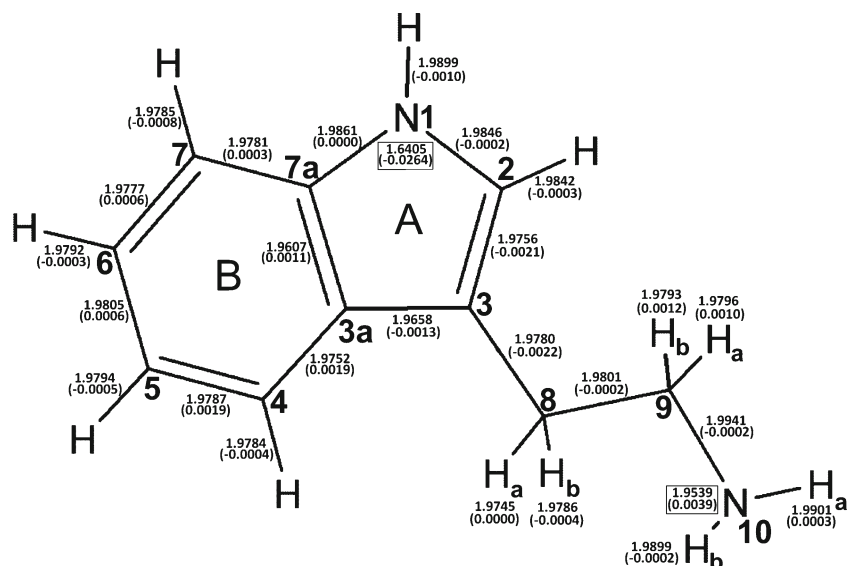
charge transfers from $\sigma_{C9—Ha}$ bonding orbital decreased in −6.44 %, and $E^{(2)}$ sums from $\sigma_{C9—Hb}$ decreased in −6.69 % in solution (Table S4a and Fig. 7). Bond lengths, bond polarization, and electron density at BCP and at NCP changed slightly following N—H trends.

Solvent effects on MEPs at N_1 and N_{10}

Augmented reactivity at N_1 site in solution found by MEP (Fig. 2) was explained by the relevant donor ability of N_1—H, effect that was improved in solution (i). These changes were also correlated with increased population in pyrrole ring and increased natural charge of N_1 (Figs. 4 and 5).

Augmented reactivity at N_{10} site in solution was explained by the donor ability of their lone pair, which decreased in solution (vi). These changes were associated with the increased lone pair population (Fig. 4) and increased natural

charge at N_{10} (Fig. 5) and also with an expected decrease in p-character (1.35 % for A^+TG^- conformer).

Solvent effects on MEPs at ring B

The net charge in vacuum and in solution for A^+TG^- conformer in each moiety is also shown in Fig. 5. It is worth noting that main charge transfers occurred from ring B and side chain to ring A in vaccum, but in solution the main charge displacement occurred from side chain and ring A to ring B.

These results can be related to specific charge transfers. In fact, relevant charge transfers taking charge from ring A to ring B, and from ring B to ring A in vacuum and in solution are shown in Table 5. The sums are displayed in Fig. 6 (see filled arrows). We quantified charge transfer from ring A to ring B, which was related to an energy of hyperconjugative interactions of 74.01 kcalmol^{-1} in solution, and of 72.18 kcal

Fig. 5 NBO analysis of natural charge of carbon, hydrogen and nitrogen atoms for A^+TG^- conformer in vacuum (values in parenthesis account for the difference of natural charge values between the structures in aqueous solvent and gas phase). The values of the sum of natural charge by fragment (benzene ring, pyrrole ring and sidechain) in vacuum/solvent are also shown
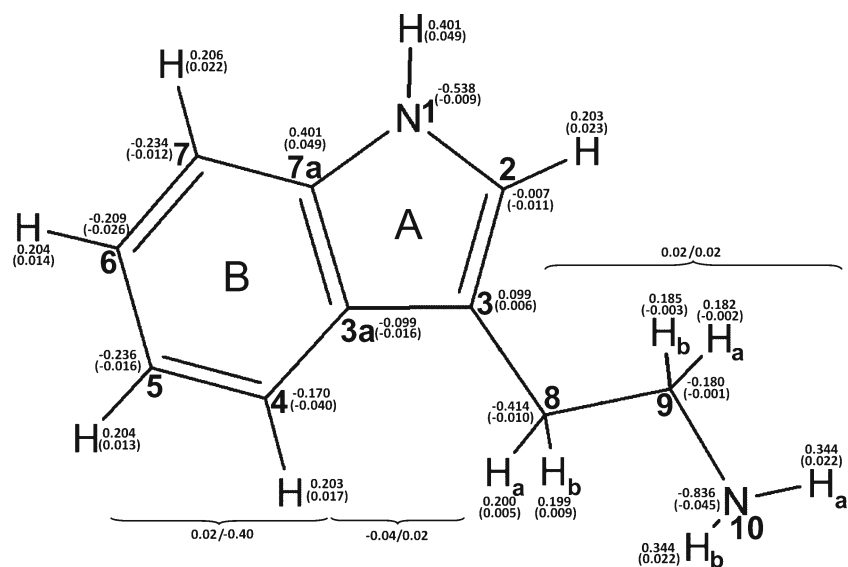
Fig. 6 Charge delocalization for A$^+$TG$^-$ conformer. Dashed arrows represent charge delocalization mechanisms taking charge from C—H bonds, N—H bonds and sidechain to A and B rings. Top right shows the sum of second-order stabilization energies, E$^{(2)}$, in vacuum for charge delocalization from ring A to ring B and vice versa. Values in parenthesis account for the difference of E$^{(2)}$ sum values between the structures in aqueous solvent and gas phase
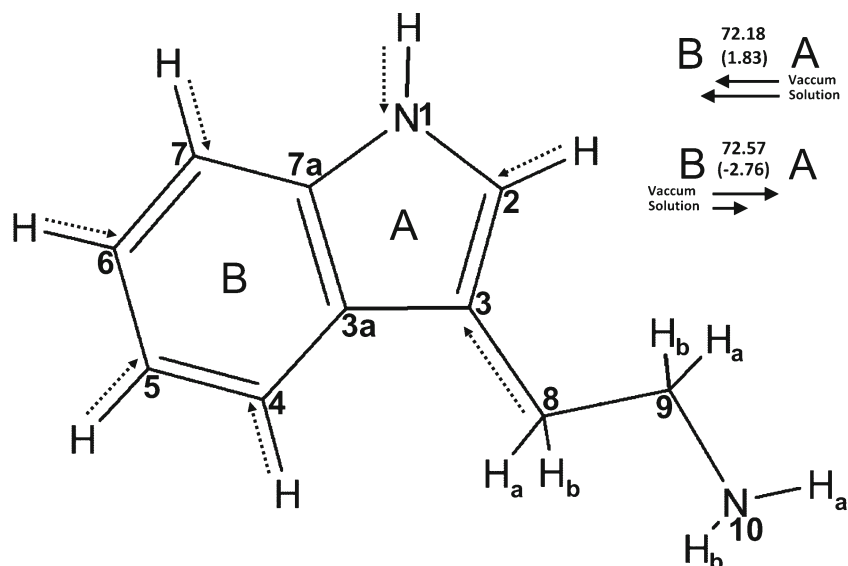
mol^{-1} in vacuum. The charge transfer from ring B to ring A was related to an energy of 69.81 kcal mol^{-1} in solution and of 72.57 kcal mol^{-1} in vacuum. Therefore, our results showed a net charge transfer from A to B in solution accounting for an energy of hyperconjugative interactions of 4.20 kcal mol^{-1}. In vacuum the net charge transfer was from B ring to A ring, and the corresponding energy was only 0.39 kcal mol^{-1}. According to these results we drew the conclusion that in vacuum the net charge delocalization was slight, and went from ring B to A, and in solution the net delocalization was
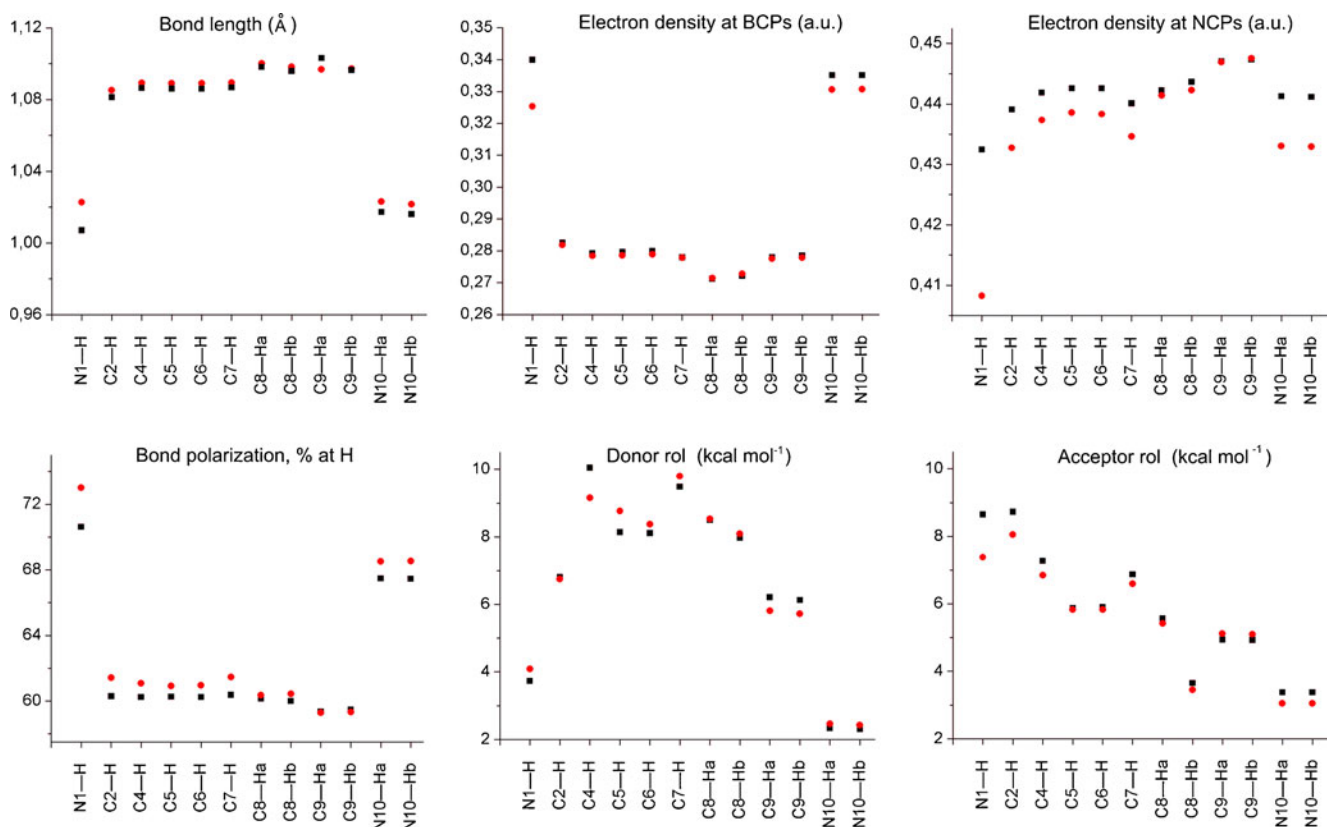
Fig. 7 Relevant changes in bond lengths, electron density at NCP of hydrogen atom, electron density at BCPs, bond polarization (% electron density at H atom), donor ability, and acceptor ability of C—H and N—H bond orbitals belonging to A$^+$TG$^-$ conformer when the solvent effect is considered. Red circles (black squares) correspond to values in aqueous solution (in vacuum)

higher and went from A ring to B ring, thus showing an inversion and enhancement of the electron delocalization mechanisms in solution.

For example, for conformer A^+TG^- an increase in 36.74 % of transfers taking charge from ring A to ring B was found, and a decrease in 26.96 % of charge transfers taking charge from ring B to ring A was found (Table 5). These changes were interestingly related to the increased donor ability of C_2—C_3 and the increased acceptor ability of C_5—C_6 and C_4—C_5 bonds shown in Table 4, and with a decrease in populations of $\sigma_{C2—C3}$ and $\pi_{C2—C3}$ bonding orbitals (−0.11 % and −0.52 %, respectively).

These results explain the augmented reactivity for indole rings found in solution by MEPs analysis (Figs. 2 and 3), and allows us to deepen the understanding of solvent effects on MEPs.

Molecular polarizability and dipole moment

The values of dipole moment and the isotropic molecular polarizability are of interest as an indication of the solubility and chemical reactivity of the molecules under study. Isotropic polarizability is a measure of electronic distortion in a molecule, caused by an external electric field, and a good indicator of how the total charge distribution of a molecule is affected [28].

The permanent electric dipole moment of an isolated molecule (μ) is also an important predictor of its behavior in physical, chemical, and biological processes. The dipole moment represents a generalized measure of the charge density in a molecule and is a reactivity index, which is very important to define biological properties, especially those related to interaction with the active sites of an enzyme [29]. It can be determined by a variety of techniques. Because the magnitudes and directions of the dipole moments are sensitive to molecular size and shape they can also serve as a useful tool in conformational analysis [11].

The values of the modulus of the permanent dipole moments (μ values) of TRA conformers are listed in Table 6. The observed variation allowed us to support that the values of dipole moments can be used to distinguish different TRA conformers [11].

The μ variation found by considering all conformers warns about the use of the theoretical values by considering only the most stable conformer. To properly account for the conformational landscape, a Maxwell-Boltzmann statistical average at 298.15 K of each μ cartesian component (Eqs. 3 and 4) was previously proposed [27].

Our results showed that μ average Maxwell-Boltzmann values for TRA conformers (Table 6) were higher than the μ value for the most stable conformer.

As expected, increased dipole moment values were found in solution; however, the solvent effect was not uniform.

Table 6 Values of the modulus of the permanent dipole moment for the TRA conformers calculated at B3LYP/6-31+G** level of theory in aqueous solvent and gas phase[a]

Conformer	Vacuum		Solution		Δ[c]
$A^+G^-G^+$	1.46(1.60)[d]	2.06[b]	2.28	2.98[b]	0.82
$A^+G^-G^-$	2.99(2.70)		4.50		1.51
A^+TG^-	2.80(2.60)		4.17		1.37
A^+TG^+	3.05		4.71		1.66
A^+TT	1.42		2.24		0.82
A^+G^+T	3.01		4.95		1.93
$A^+G^+G^-$	2.62(2.40)		3.71		1.10
CTG^-	1.30		2.04		0.74
CG^-T	2.33		3.00		0.67
CTG^+	2.97		4.51		1.54
CTT	2.97		4.49		1.52
$A^+G^+G^+$	2.44		3.19		0.76

[a] All values are expressed in Debye

[b] Values of the Maxwell-Boltzmann statistical averages for TRA conformers

[c] Δ represents the difference of the modulus of the permanent dipole moment for the structure in aqueous solvent and gas phase

[d] The experimental values in parenthesis are from ref. [11]

Up-conformers were previously associated with higher dipolar moments [11]. We found that other kinds of conformers showed high μ values (A^+TG^+ and A^+G^+T).

Taking into account the experimental values for $A^+G^-G^+$, $A^+G^-G^-$, A^+TG^- and $A^+G^+G^-$ (Table 6) a good reproduction of the experimental trend was observed at B3LYP/6-31+G** level. Moreover, considering some previously obtained values at MP2/6-31 G* level [11], a better description at B3LYP/6-31+G** level was found ($\Delta_{Exp\text{-} B3LYP/6-31+G**}$:

Table 7 Polarizability data for the TRA conformers calculated at B3LYP/6-31+G** level of theory in gas phase[a]

Conformer	α_{xx}	α_{yy}	α_{zz}	$<\alpha>$	Average[b]
$A^+G^-G^+$	165.94	143.89	89.22	133.02	133.51
$A^+G^-G^-$	166.64	143.95	90.21	133.60	
A^+TG^-	168.81	148.76	85.95	134.50	
A^+TG^+	166.50	148.51	85.55	133.52	
A^+TT	166.97	148.61	85.03	133.54	
A^+G^+T	163.35	148.15	88.03	133.18	
$A^+G^+G^-$	164.46	146.13	89.60	133.40	
CTG^-	176.88	143.15	80.97	133.67	
CG^-T	180.81	139.13	82.20	134.05	
CTG^+	175.74	142.75	81.14	133.21	
CTT	175.74	142.75	81.14	133.21	
$A^+G^+G^+$	162.97	154.35	84.45	133.92	

[a] All the values are expressed in a.u

[b] Maxwell-Boltzmann statistical average at 298.15 K

−0.14, 0.29, 0.20 and 0.22, and $\Delta_{Exp-MP2/6-31G*}$: −0.26, 0.32, 0.25 and 0.27 for $A^+G^-G^+$, $A^+G^-G^-$, A^+TG^- and $A^+G^+G^-$, respectively). It is worth mentioning that in aqueous phase we found the same trend as that in vacuum.

Table 7 shows values in vacuum for the polarizabilities (Eqs. 5 and 6). To the best of our knowledge, research concerning the molecular polarizabilities of TRA conformers has not yet been reported, and therefore, our results are the first prediction of them. Maxwell-Boltzmann statistical average at 298.15 K of polarizabilities of TRA conformers was 133.51 a.u., thus indicating their nature of being soluble in polar solvents, and their ability to polarize other atoms or molecules.

Conclusions

The stereochemistry of TRA was studied in aqueous solution, emphasizing the description of the factors involved. As in gas phase, 21 lowest-energy conformers were characterized. The features of the conformers in solution were similar to those obtained in gas phase, and were also classified into four groups according to the position of the amino group relative to the indole ring: *gauche* on the pyrrole (group G^-), *gauche* on the phenyl (group G^+) or *anti* related to the indole ring [groups T (with the indole ring at right angles to the C_8—C_9 bond) and T' (with the indole ring parallel to the C_8—C_9 bond)]. All structures were stabilized in solution, but relative conformational population at 298.15 K calculated with the Boltzmann distribution showed considerable variation in solution. Structural changes were related with charge delocalization mechanisms, which explained the changes found in conformational population in aqueous phase. An NBO analysis allowed us to investigate which orbital interactions are mainly useful to explain the stability order of the conformers observed in solution.

Intramolecular interactions were studied and characterized by the theory of atoms in molecules, characterizations of bonding interactions being similar to those in vacuum. The AIM analysis also allowed us to identify and characterize intramolecular hydrogen bonding (HB) interactions in solution and the effect of the solvent on them.

From an AIM/NBO analysis the solvent effects on chemical bonds were described and quantified. For X—H bonds we found increased bond length, bond polarization and donor ability and decreased ρ at BCP and at NCP of H atom, and also decrease in their acceptor ability. The changes were higher for X—H bonds attached to highly polarizable π-systems. Changes on lone pairs were also addressed.

We concluded that in all conformers in both gas phase and aqueous phase there were three main sites of electrophilic attack associated with C_5, N_1 and N_{10} atoms. Moreover, by a deep analysis of molecular electrostatic potential we explained the increased reactivity in solution through specific charge delocalization mechanisms.

The results also allowed us to conclude that in vacuum the net charge delocalization between ring A and ring B was slight and went from ring B to ring A, and in solution the net delocalization was higher and went from ring A to ring B, thus showing an inversion and enhancement of specific electron delocalization mechanisms in solution. We also described and quantified charge delocalization mechanisms taking charge from C—H bonds, N—H bonds and sidechain to A and B rings in aqueous solution.

Solvent effects on MEPs at N—H and C—H chemical bonds were also quantified and rationalized by charge delocalization mechanisms, thus connecting changes in MEPs with changes in structure, bonds polarization, orbital bonding populations, natural charges and bond topological properties.

Taking into account the experimental values of μ a good reproduction of the experimental trend was observed at B3LYP/6-31+G** level.

Up-conformers have been previously associated with higher dipolar moments, but we concluded that not only *up*-conformers have the higher μ values.

Our results also showed μ mean Maxwell-Boltzmann value for TRA conformers higher than the μ value for the most stable conformer, thus showing that if the prediction of μ value is performed considering only the most stable conformer the μ value will be underestimated. Moreover, to the best of our knowledge, research concerning the molecular polarizabilities of TRA conformers has not yet been reported, and therefore, our results are the first prediction of them and led to propose TRA as a molecule soluble in polar solvents with the ability to polarize other atoms and molecules.

References

1. Khan MTH (2007) Bioactive heterocycles V. Springer, Berlin, pp 145–154
2. Bozkaya P, Dogan B, Suzen S, Nebioglu D, Ozkan SA (2006) Determination and investigation of electrochemical behaviour of 2-phenylindole derivatives: discussion on possible mechanistic pathways. Can J Anal Sci Spectr 51:125–139
3. Kruk I, Aboul-Enein HY, Michalska T, Lichszteld K, Kubasik-Kladna K, Olgen S (2007) In vitro scavenging activity for reactive

oxygen species by N-substituted indole- 2-carboxylic acid esters. J Lumin 22:379–386

4. Poeggeler B, Thuermann S, Dose A, Schoenke M, Burkhardt S, Hardeland R (2002) Melatonin's unique radical scavenging properties—roles of its functional substituents as revealed by a comparison with its structural analogs. J Pineal Res 33:20–30

5. Shirinzadeh H, Eren B, Gurer-Orhan H, Suzen S, Özden S (2010) Novel Indole-Based Analogs of Melatonin: synthesis and in vitro antioxidant activity studies. Molecules 15:2187–2202

6. Böhm M, Brause R, Jacoby C, Schmitt M (2009) Conformational relaxation paths in tryptamine. J Phys Chem A 113:448–455, references cited therein

7. Lobayan RM, Pérez Schmit MC, Jubert AH, Vitale A (2011) Conformational and stereoelectronic investigation of tryptamine. An AIM/NBO study. J Mol Mod 18:2577–2588

8. Peteanu LA, Levy DH (1988) Spectroscopy of complex of tryptamine and 3-indolepropionic acid with various solvents. J Phys Chem 92:6554–6561

9. Sipior J, Sulkes M (1988) Spectroscopy of tryptophan derivatives in supersonic expansions: Addition of solvent molecules. J Chem Phys 88:6146–6156

10. Carney JR, Dian BC, Florio GM, Zwier TS (2001) The role of water bridges in directing the conformational preferences of 3-indolepropionic acid and tryptamine. J Am Chem Soc 123:5596–5597

11. Nguyen TV, Pratt DW (2006) Permanent electric dipole moments of four tryptamine conformers in the gas phase: a new diagnostic of structure and dynamics. J Chem Phys 124:54317–54323

12. Klene M, Li X, Knox JE, Hratchian HP, Cross JB, Adamo C, Jaramillo J, Gomperts R, Stratmann RE, Yazyev O, Austin AJ, Cammi R, Pomelli C, Ochterski JW, Ayala PY, Morokuma K, Voth GA, Salvador P, Dannenberg JJ, Zakrzewski VG, Dapprich S, Daniels AD, Strain MC, Farkas O, Malick DK, Rabuck AD, Raghavachari K, Foresman JB, Ortiz JV, Cui Q, Baboul AG, Clifford S, Cioslowski J, Stefanov BB, Liu G, Liashenko A, Piskorz P, Komaromi I, Martin RL, Fox DJ, Keith T, Al-Laham MA, Peng CY, Nanayakkara A, Challacombe M, Gill PMW, Johnson B, Chen W, Wong MW, Gonzalez C, Pople JA (2003) Gaussian03, Revision B.02. Gaussian Inc, Pittsburgh

13. Barone V, Cossi M (1998) Quantum calculation of molecular energies and energy gradients in solution by a conductor solvent model. J Phys Chem A 102:1995–2001

14. Becke AD (1993) Density-functional thermochemistry. III. The role of exact exchange. J Chem Phys 98:5648–5652

15. Lee C, Yang W, Parr RG (1988) Development of the Colle-Salvetti correlation energy formula into a functional of the electron density. Phys Rev B 37:785–789

16. Flúrkiger P, Lúthi HP, Portmann S, Weber J (2000) MOLEKEL 4.0. Swiss Center for Scientific Computing, Manno, Switzerland

17. Biegler-Köning FW, Bader RFW, Tang TH (1982) Calculation of the average properties of atoms in molecules. II. J Comput Chem 3:317–328

18. Glendening ED, Reed AE, Carpenter JE, Weinhold F NBO 3.1 (2003) Program as implemented in the Gaussian 03 package

19. Alabugin IV, Zeidan TA (2002) Stereoelectronic effects and general trends in hyperconjugative acceptor ability of σ bonds. J Am Chem Soc 124:3175–3185

20. Bader RFW (1995) Atoms in molecules. A quantum theory. Oxford University Press, Oxford

21. Politzer P, Truhlar DG (eds) (1981) Chemical applications of atomic and molecular electrostatic potentials. Plenum, NY

22. Politzer P, Murray JS (1991) Theoretical biochemistry and molecular biophysics: a comprehensive survey. In: Beveridge DL, Lavery R (eds) Protein, vol 2. Adenine, Schenectady, pp 165–191

23. Roy DK, Balanarayan P, Gadre SR (2009) Signatures of molecular recognition from the topography of electrostatic potential. J Chem Sci 121:815–821

24. Lobayan RM, Jubert AH, Vitale MG, Pomilio AB (2009) Conformational and electronic (AIM/NBO) study of unsubstituted A-type dimeric proanthocyanidin. J Mol Model 15:537–550

25. Bentz EN, Jubert AH, Pomilio AB, Lobayan RM (2010) Theoretical study of Z isomers of A-type dimeric proanthocyanidins substituted with R=H, OH and OCH3: stability and reactivity properties. J Mol Mod 16:1895–1909

26. Pérez Schmit MC, Jubert A, Vitale A, Lobayan RM (2010) Electronic structure and conformational properties of 1 H-indole-3-acetic acid. J Mol Mod 17:1227–1239

27. Lobayan ML, Bentz EN, Jubert AH, Pomilio AB (2012) Structural and electronic properties of Z isomers of $(4\alpha \rightarrow 6'', 2\alpha \rightarrow O \rightarrow 1'')$-phenylflavans substituted with R=H, OH and OCH3 calculated in aqueous solution with PCM solvation model. J Mol Mod 18:1667–1676

28. Weber KC, Honório KM, Bruni AT, da Silva ABF (2006) The use of classification methods for modeling the antioxidant activity of flavonoid compounds. J Mol Model 12:915–920

29. Olivero-Verbel J, Pacheco-Londoño L (2002) Structure-activity relationships for the anti-HIV activity of flavonoids. J Chem Inf Comput Sci 42:1241–1246